JOURNAL OF SOLID STATE CHEMISTRY 57, 323–331 (1985)

Electrochemical Intercalation and Deintercalation of Na_xMnO_2 Bronzes

A. MENDIBOURE, C. DELMAS, AND P. HAGENMULLER

Laboratoire de Chimie du Solide du CNRS, Université de Bordeux I, 351 cours de la Libération–33405 Talence Cedex, France

Received July 24, 1984; in revised form October 21, 1984

Various Na_xMnO_2 bronzes have been electrochemically deintercalated. $Na_{0.40}MnO_2$ has a channel structure which is maintained for a large intercalation range ($0.30 \leq x \leq 0.58$). In order to explain the upper intercalation limit, an ordered sodium distribution between two types of Na^+ sites is proposed. $Na_{0.70}MnO_2$ and α-$NaMnO_2$ have lamellar structures of P2 and O'3 types. During intercalation the original P2 type is maintained for $0.45 \leq x \leq 0.85$ while two reversible structural transitions are observed from α-$NaMnO_2$. A similar behavior occurs during the deintercalation of the high-temperature β-$NaMnO_2$ variety. In each case of the structural transition the double octahedral layers remain unchanged. Electronic localization (increased by Mn^{3+} Jahn–Teller effect) tends to trap the Na^+ ions and therefore increases the relaxation time of the investigated materials.

I. Introduction

Investigation of the crystal chemistry of the Na_xMnO_2 system by classical high-temperature synthesis has shown the existence of several phases in the range $0 \leq x \leq 1$ (*1*). Their compositions are given in Fig. 1. Structures are three-dimensional for the lower x values and two-dimensional for the higher ones.

Many studies have been devoted to intercalation–deintercalation from Na_xMO_2 phases (*2–4*). These materials are metallic or semiconducting, depending on the M–M distance and *d*-orbital overlap. As the intercalation kinetics are strongly dependent on this type of behavior, the occurrence of an electronic localization due to the Jahn–Teller effect of manganese (+ III) led us to study intercalation processes in Na_xMnO_2 phases. A general survey of the structures of the investigated materials is given below.

Structures of the Starting Phases

(a) 3D Structures

In $Na_{0.40}MnO_2$ and $Na_{0.44}MnO_2$, files of edge-sharing MnO_6 octahedra are linked so as to form channels in which the sodium ions are intercalated. $Na_{0.40}MnO_2$ is isostructural with psilomelane $(Ba,H_2O)_2Mn_5O_{10}$ (Fig. 2) whose structure was described by Wadsley (*5*). Considering the large size of the channels, in $Na_{0.40}MnO_2$ the intercalation and deintercalation of sodium should be possible. The exact site of sodium within the tunnels is not well known. Hence it was interesting to determine the highest x value accessible from $Na_{0.40}MnO_2$ by electrochemical intercalation in an attempt to precisely locate the alkali ion site.

The occurrence of two types of manganese sites in $Na_{0.44}MnO_2$ (octahedral and rectangular pyramidal) could make a hop-

0022-4596/85 $3.00

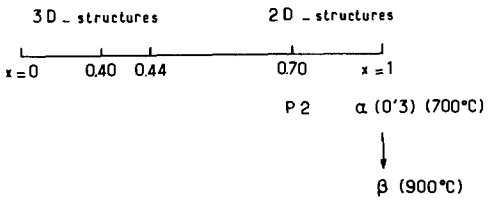

FIG. 1. Na_xMnO_2 phase compositions.

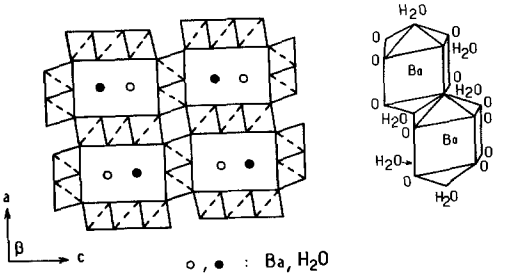

FIG. 2. Psilomelane structure of $(Ba,H_2O)_2Mn_5O_{10}$ (5).

ping mechanism difficult and thereby decrease the electronic conductivity. As a consequence intercalation has not been tested in this material.

(b) 2D phases

$Na_{0.70}MnO_{2+y}$ and α-NaMnO₂. For higher sodium contents ($x > 0.50$) lamellar structures have been found. These lamellar structures are composed of MnO_2 sheets, built up of edge-sharing MnO_6 octahedra. The structure of $Na_{0.70}MnO_{2+y}$ is called P2 type with an *ABBA* oxygen stacking (Fig. 3). In the convention used to designate the structural type, the letter O or P stands for the alkali site (octahedral or prismatic) and the number gives the number of sheets contained in the unit cell. α-$NaMnO_2$ has an O'3 structure (*ABCABC* oxygen stacking (Fig. 3)). In O'3, the prime symbol indicates a monoclinic structural distortion with respect to the hexagonal lattice.

β-$NaMnO_2$. This high-temperature phase also exhibits a layer structure, but the MnO_2 sheets are completely different from those mentioned above. They constitute a double stack of edge-sharing MnO_6 octahedra. Between two neighboring sheets the sodium ions occupy octahedral sites (Fig. 4). As for other A_xMO_2 sheet structures, it is possible to imagine sheet displacements leading to various alkali ion environments. The possible sites, depending on the relative positions of the MO_2 sheets, are either

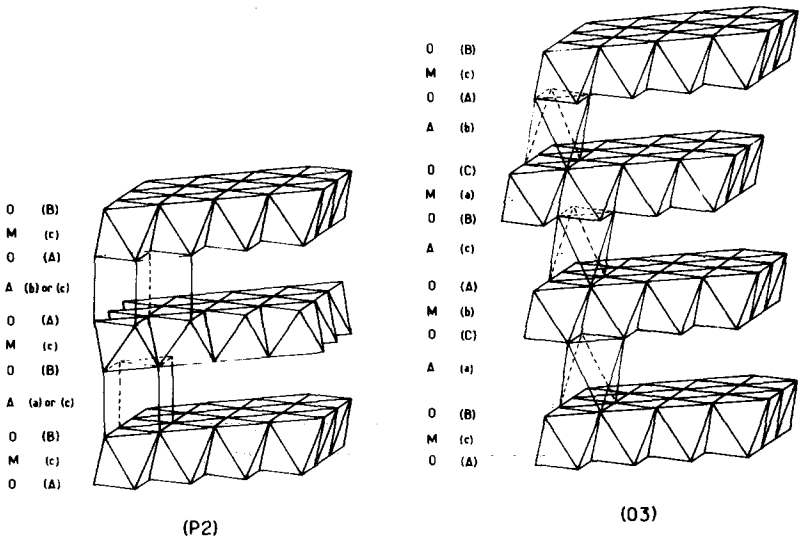

FIG. 3. $Na_{0.7}MnO_2$(P2) and α-$NaMnO_2$ (O'3) structures.

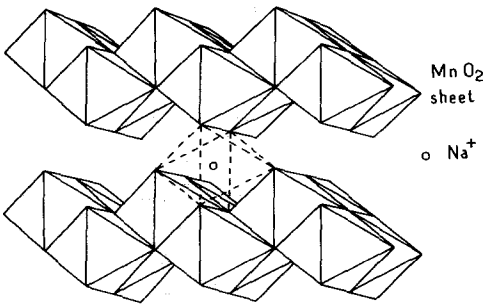

FIG. 4. β-$NaMnO_2$ structure.

octahedral, trigonal prismatic (TP), or rectangular prismatic (RP). Such an environment for the alkali element has been reported for materials like $Rb_xM_yTi_{2-y}O_4$ (RP) or $K_xM_yTi_{2-y}O_4$ (TP) (*6*).

II. Experimental

All the starting materials have been synthesized from mixtures of Na_2O, MnO_2, and Mn_2O_3 according to the preparation conditions given by Parant *et al.* (*1*).

To perform the intercalation and deintercalation of sodium, galvanostatic charge and discharge of the following chain were carried out:

sodium | liquid electrolyte | Na_xMnO_2 + graphite.

A $NaClO_4$ (1 *M*) solution in propylene carbonate was used as the electrolyte. The deintercalation limit was given by the upper stability limit of the liquid electrolyte (3.5 V vs sodium). Conductivity measurements in good agreement with literature values (*1*) indicated a semiconductor behavior for $Na_{0.40}MnO_2$, $Na_{0.70}MnO_2$, and α-$NaMnO_2$. Thus, graphite was added (up to 50% by weight) to the materials studied in order to diminish the resistance of the positive electrode. A data processing system managed all the cell testings (*7*). The materials recovered at different steps of the cycling have been studied by X-ray diffraction.

III. Results and Discussion

(*a*) $Na_{0.40}MnO_2$

Figure 5 shows a cycling curve of a cell using $Na_{0.40}MnO_2$ as a positive electrode. The continuous variation of the voltage during the intercalation (or deintercalation) and the X-ray diffraction data show the existence of a solid solution in the range $0.30 \leq x \leq 0.58$. The deintercalation could not be performed below $x = 0.30$ because of the electrolyte instability at high cell voltages. The maximum intercalation should correspond to the filling of all available sites for the sodium ions. However, if the material is discharged below 2 V ($x \geq 0.50$), the following charge is impossible to perform due to a very high resistance to sodium removal. However, a continuous discharge of the cell leads to a maximal x value of about 0.58.

Comparison of the X-ray diffraction patterns shows unambiguously that the unit cell parameters are modified during the intercalation process. Nevertheless, as only some diffraction lines are affected and as the material crystallizes in the monoclinic system, refinement of the unit cell parameters does not lead to significant results.

The upper intercalation limit gives worth-

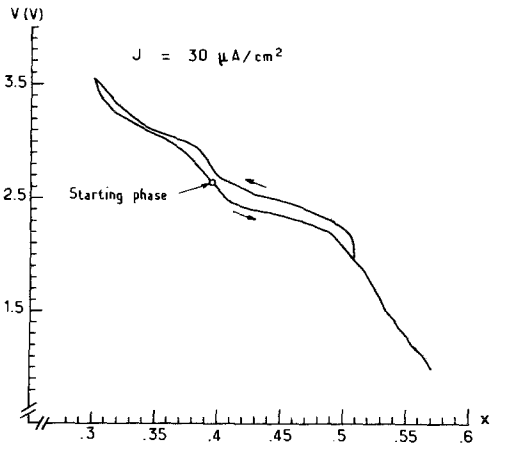

FIG. 5. Electrochemical cycling from $Na_{0.40}MnO_2$.

while information in an attempt to identify the exact site of the sodium ions. If we consider $(Ba,H_2O)_{0.40}MnO_2$, which is isostructural with $Na_{0.40}MnO_2$, the barium ions are in 10-coordinated sites (six oxygen atoms and four water molecules (Fig. 2)). It is highly improbable that sodium ions could replace both Ba and H_2O; this would result in strong electrostatic repulsions destabilizing the structure.

It is possible to imagine two possible sites for the alkali ions:

—Sites of C.N.5 (rectangular pyramids) are available at the corners of the channels (Fig. 6). If they were all occupied the composition would be $Na_{0.80}MnO_2$.

—The second possible sites for sodium are trigonal prismatic (Fig. 6). Their filling would also lead to the formulation $Na_{0.40}MnO_2$.

Thus, if the sodium ions occupy both pyramidal and prismatic sites, the border limit formula would be $Na_{1.20}MnO_2$. As both sites are sharing rectangular faces, they cannot be filled simultaneously. But the occupancy of half of them leads to the composition $Na_{0.60}MnO_2$ which is the experimentally observed limit. Furthermore, some MnO_6 octahedra share two faces with two pyramidal sites. If one of the pyramids is occupied, the strong electrostatic repulsion $Mn^{n+} \leftrightarrow Na^+$ shifts the Mn ion from its normal position and decreases the probability that the second pyramid will be occupied. As a result an ordered occupation of the sites can be assumed for the upper value of x, as proposed in Fig. 6.

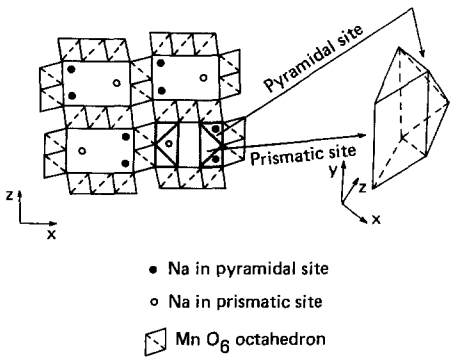

FIG. 6. Sodium distribution in rectangular pyramidal and trigonal prismatic sites proposed for the composition $Na_{0.60}MnO_2$.

As only a definite composition is observed by high-temperature synthesis, a sodium ordered distribution would also exist in the starting phase $Na_{0.40}MnO_2$. Two assumptions can be made: the sodium can fill either all of the prismatic or half of the pyramidal sites. The first hypothesis, which lowers the electrostatic interactions, seems to be the most probable. A two-phase domain is not observed; so a progressive change in the Na^+ distribution should occur during intercalation for $x \geq 0.40$. Such a behavior could account for the slope change in the electrochemical curve observed for $x = 0.40$.

(*b*) $Na_{0.70}MnO_{2+y}$

Parant *et al.* have shown that the general formula of the P2-type phase was $Na_{0.70}MnO_{2+y}$. y varies with the synthesis conditions (temperature and oxygen pressure). Density measurements have shown that the crystallographic formula is actually $Na_{0.70}(2/(2 + y))\,Mn(2/2 + y))O_2$ (*8*). Due to the Jahn–Teller effect of trivalent manganese, an orthorhombic distortion is observed, except for the higher values of y where the amount of trivalent manganese is too small to induce a macroscopic distortion. To simplify our investigation, all electrochemical measurements have been done from the hexagonal phase of composition $Na_{0.70}MnO_{2.25}$.

The cycling curve obtained under a current density of 70 $\mu A/cm^2$ is shown in Fig. 7. The electrochemical behavior and the X-ray diffraction study show the existence of a solid solution in the range $0.45 \leq x \leq 0.85$. Although the amount of trivalent manganese increases during intercalation, the P2 structural type is maintained without crystallographic distortion.

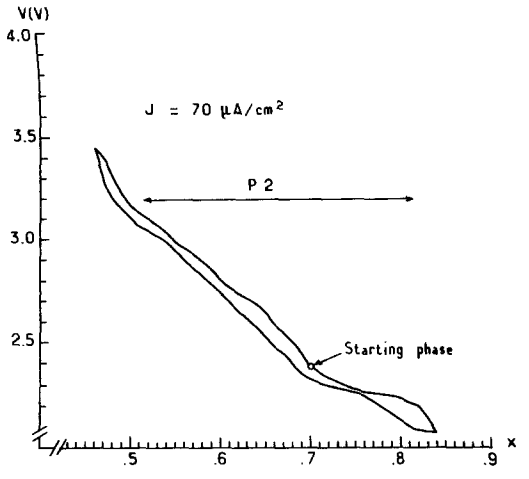

FIG. 7. Electrochemical cycling from $Na_{0.70}MnO_{2.25}$(P2).

As for $Na_{0.40}MnO_2$, if the cell is deeply discharged below 2.0 V, the following charge is impossible to perform, due to a very high resistance to Na^+ removal. Thus cycling curves do not go below 2.0 V.

The parameter variation of the hexagonal cell is given in Fig. 8. During deintercalation, the *c* parameter, perpendicular to the MnO_2 sheets, increases notably while the *a* parameter, corresponding to the Mn–Mn distance within the sheets, decreases. The decrease in sodium leads to an increase in the repulsive forces between the MO_2 sheets. The result is an increase in the intersheet distance.

In the same way the mean oxidation state of manganese ions increases with decreasing x; the lower ionic radius of Mn^{+IV} with respect to Mn^{+III} leads to higher covalency of the manganese–oxygen bonds and as a consequence to decrease of the *a* parameter.

Such an evolution of the *c* and *a* parameters during alkali ion deintercalation has been previously observed for all Na_xMO_2 systems (*2–4, 9*). As in the similar Na_xCoO_2 (P2) system no structural transition is observed. This result is consistent with the impossibility of obtaining a reversible transition between a P2-type structure and an O3- or P3-type structure without breaking *M*–O bonds, which must be excluded at such a low temperature.

Compared relaxation of $Na_{0.70}MnO_{2+y}$ and $Na_{0.70}CoO_2$. The $Na_{0.70}MnO_{2.25}$ phase is isostructural with $Na_{0.70}CoO_2$. The two materials differ only in their electronic behavior. While the former is a semiconductor (activation energy = 0.34 eV), the second one exhibits metallic character. As a result it is interesting to compare the relation between sodium diffusion kinetics and electronic properties of both materials.

In the current-pulse relaxation technique a short constant current pulse is used to inject or to remove sodium ions from the positive electrode. The chemical diffusion coefficient of sodium is calculated from the decay rate of the resulting transient voltage.

Figure 9 shows the evolution of the potential vs time relationship during relaxation for both materials. The current pulse was about 5.6 mA during 15 sec. It can be emphasized that the return to the open circuit potential was much faster in the case of $Na_{0.70}CoO_2$ than for $Na_{0.70}MnO_{2.25}$. The diffusion coefficients of sodium have been calculated assuming the following relaxation law (*10*):

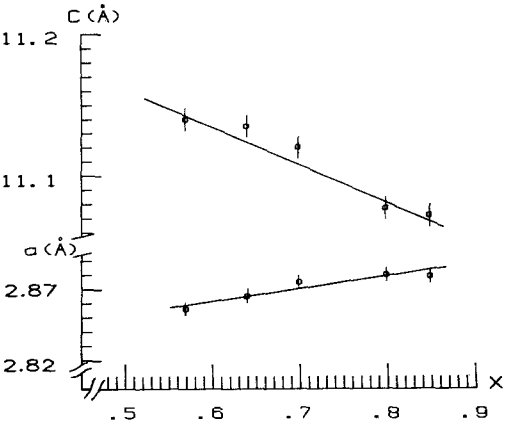

FIG. 8. Unit cell parameter variation during intercalation and deintercalation from $Na_{0.70}MnO_{2.25}$.

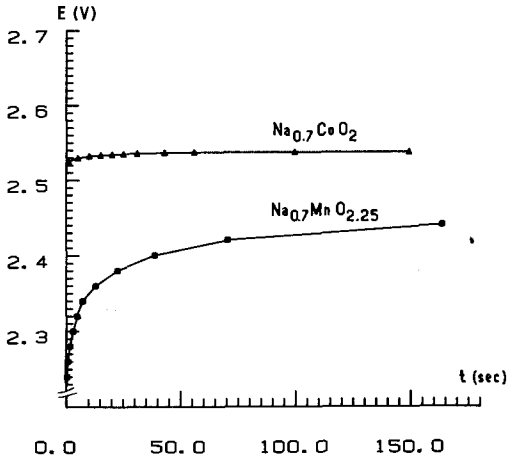

FIG. 9. Relaxation curves for Na_xMO_{2+y} (M = Mn, Co)(P2) phases.

$$\frac{E_0 - E}{RT} = \frac{I\Delta t}{F^2C(1-y)\sqrt{\pi Dt}}$$

R = gas constant
T = absolute temperature
F = Faraday constant
I = pulse intensity
Δt = pulse duration
C = final concentration of the charge carriers
$1 - y$ = occupancy rate of available sites in the structure: $y = x/x_{max}$.

This law, valid only for the Nernst-type systems, can nevertheless give a good idea of the diffusion coefficient of the mobile ion within the host structure. The $E_0 - E = f(t^{-1/2})$ curves (E_0 = O.C. voltage, E = instantaneous potential, t = time) are linear for the last part of the relaxation (Figs. 10a and b). The nonlinearity of the first part can be attributed to an "electrolyte effect" (*10*). The following diffusion coefficients are then obtained:

$Na_{0.70}MnO_{2.25}$: $D \simeq 1.7 \times 10^{-14}$ cm$^2 \cdot$ sec^{-1}

$Na_{0.70}CoO_2$: $D \simeq 5 \times 10^{-12}$ cm$^2 \cdot$ sec^{-1}.

For $Na_{0.70}MnO_{2.25}$ we can assume a conduction mechanism by hopping ($Mn^{3+} \leftrightarrow Mn^{4+}$). The Jahn–Teller effect due to manganese$^{(+III)}$ should also increase the electronic localization. If the displacements of the two carrier types (e^- and Na^+) are coupled, this localization could explain the limitation of the ion diffusion in $Na_{0.70}MnO_{2.25}$. In $Na_{0.70}CoO_2$ the metallic behavior emphasizes the electronic delocalization, making much easier the ion diffusion.

(*c*) *α-NaMnO₂*

Figure 11a shows the cycling curve ob-

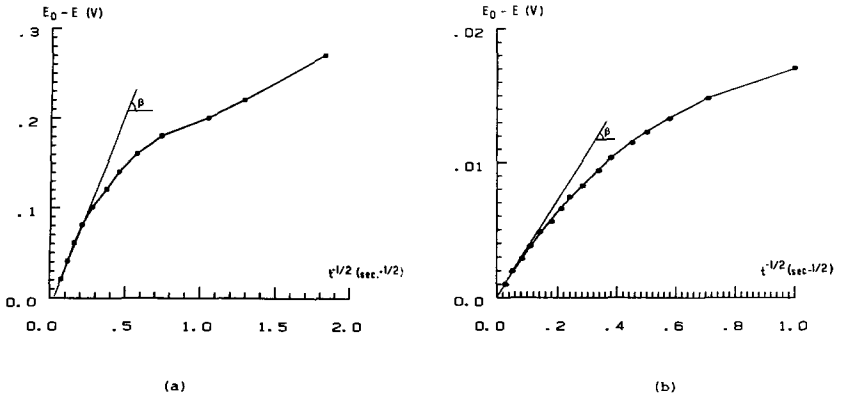

FIG. 10 $E_0 - E = f(1/\sqrt{t})$ curves for $Na_{0.70}MnO_{2.25}$ (a) and $Na_{0.70}CoO_2$ (b) tg β has been used for diffusivity calculation.

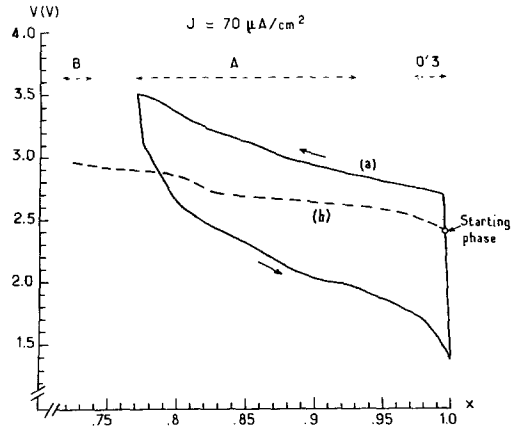

FIG. 11. Electrochemical cycling from α-$NaMnO_2$ (a); O.C. voltage curve from α-$NaMnO_2$ (b).

tained with a current density of 70 $\mu A/cm^2$ from α-$NaMnO_2$ as starting material. For a given x value the difference between the charge and discharge potential is very large. This results from the high resistivity of the material. Conductivity studies indicated that α-$NaMnO_2$ is a semiconductor with an activation energy of 0.45 eV. The intrinsic Na^+ conductivity should be very small due to the unfavorable octahedral environment (*11*). Furthermore the a/b ratio of the lattice parameters (Table I) characterizes an important Jahn–Teller effect in the MnO_6 octahedra, due to manganese(III) (ideal value of $a/b = \sqrt{3}$). As discussed above, this effect should decrease the Na^+ diffusion coefficient even more.

To observe possible plateaus in the potential, an open circuit voltage curve has been recorded (Fig. 11b). The curve shape and the X-ray diffraction studies showed

TABLE I

α-$NaMnO_2$ LATTICE PARAMETERS (*1*)

a = 5.53 Å b = 2.860 Å c = 5.77 Å β = 112.9°	$a/b \simeq 1.97$

the occurrence of two deintercalated phases A and B separated by two phase domains.

The composition of the A phase ranges from $Na_{0.93}MnO_2$ to $Na_{0.77}MnO_2$. The B phase appears at about $Na_{0.73}MnO_2$. These compositions could not be accurately determined, due to the very slow relaxation of the material. The X-ray diffraction spectra of both materials (A,B) could not be indexed. However, they are characteristic of sheet structures. Furthermore, the two structural transitions are reversible, which emphasizes the fact that the MnO_2 sheets are not destroyed during deintercalation. The Mn–O bonds are too strong to be reversibly broken and reconstituted at room temperature.

Figure 12 shows the variation of the intersheet distance obtained from the first diffraction line of the X-ray spectra. The evolution has to be compared to the intersheet distances observed for other related A_xMO_2 materials. Figure 12 shows that a trigonal prismatic environment can be assumed for the A phase. On the contrary the very large intersheeet distance observed for the B phase remains unexplained.

(*d*) β-$NaMnO_2$

Figure 13 gives the cycling curve of a cell

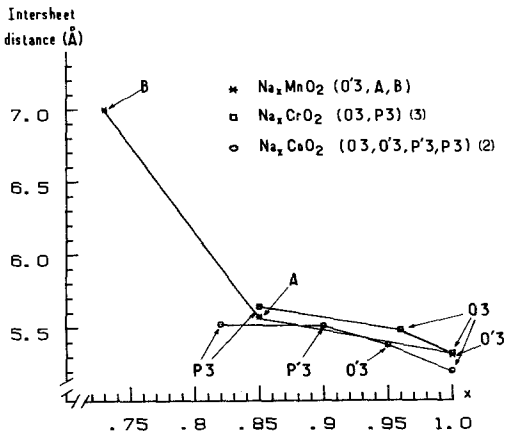

FIG. 12. Intersheet distance for the Na_xMO_2 phases.

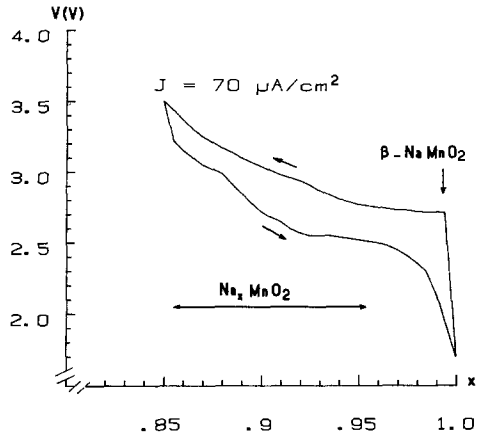

FIG. 13. Electrochemical cycling from β-$NaMnO_2$.

using β-$NaMnO_2$ as the positive electrode. When charging at 2.7 V vs. sodium, a two-phase domain is observed. It corresponds to a reversible structural transition between the starting compound β-$NaMnO_2$ and the upper limit of a solid solution ($0.85 \leq x \leq 0.96$). The X-ray diffraction pattern of this new phase has been indexed in the orthorhombic system. The unit cell parameters of the $Na_{0.91}MnO_2$ phase are given in Table II and compared to those of the starting β phase. The X-ray diffraction pattern of $Na_{0.91}MnO_2$ is given in Table III.

Since the structural transition is reversible, it can be assumed that MnO_2 double octahedral layers are maintained. The *b* parameter, which represents the intersheet distance, increases from 6.31 Å in β-$NaMnO_2$ to 7.12 Å in $Na_{0.91}MnO_2$. Such an increase is similar to that observed for other sheet oxides as a result of deintercalation (*2–4, 9*).

The values of the *a* and *c* parameters which represent the diagonal and the edge of a MnO_6 octahedron suggest a lower distortion in the deintercalated phase than in the starting one ($a/c = \sqrt{2}$ in a nondistorted octahedron).

TABLE II

UNIT CELL PARAMETERS OF RELATED β-$NaMnO_2$ PHASES

	$Na_{0.91}MnO_2$	β-$NaMnO_2$ (*1*)
$a \pm 0.006$ Å	4.052	4.770
$b \pm 0.01$ Å	7.12	6.31
$c \pm 0.004$ Å	2.984	2.852
a/c	1.36	1.67

TABLE III

X-RAY DIFFRACTION PATTERN OF $Na_{0.91}MnO_2$ RESULTING OF Na DEINTERCALATION FROM β-$NaMnO_2$

h k l	d_{obs}(Å)	d_{calc}(Å)	$I/I_{0_{obs}}$
0 1 0	7.09	7.12	vS
1 1 0	3.513	3.521	vw
0 1 1	2.745	2.752	w
1 2 0	2.671	2.674	m
1 0 1	2.404	2.403	m
1 1 1	2.266	2.277	w
2 0 0	2.031	2.026	S
1 2 1	1.996	1.992	S
0 3 1	1.861	1.858	w
0 4 0	1.780	1.780	w
2 0 1	1.675	1.676	w
0 5 0	1.424	1.424	m

Acknowledgments

The authors acknowledge the financial support of the Energy Conservation Program of EEC.

References

1. J. P. PARANT, R. OLAZCUAGA, M. DEVALETTE, C. FOUASSIER, AND P. HAGENMULLER *J. Solid State Chem.* **3**, 1 (1971).
2. C. DELMAS, J. J. BRACONNIER, C. FOUASSIER, AND P. HAGENMULLER, *Solid State Ionics*, **3–4**, 165 (1981).
3. J. J. BRACONNIER, C. DELMAS, AND P. HAGENMULLER, *Mater. Res. Bull.* **17**, 993 (1982).
4. A. MAAZAZ, C. DELMAS, AND P. HAGENMULLER, *J. Inclusion Phenom.* **1**, 45 (1983).
5. A. D. WADSLEY, *Acta Crystallogr.* **6**, 433 (1953).
6. D. GROULT, C. MERCEY, AND B. RAVEAU, *J. Solid State Chem.* **32**, 289 (1980).

7. A. MENDIBOURE AND C. DELMAS, *Computers and Chemistry,* in press.
8. C. DELMAS AND C. FOUASSIER, *Z. Anorg. Allg. Chem.,* **420,** 184 (1976).
9. C. DELMAS, J. J. BRACONNIER, C. FOUASSIER, AND P. HAGENMULLER, *Z. Naturforsch. B* **36,** 1368 (1981).
10. A. LE MEHAUTE, Thesis, University of Nantes (1979).
11. C. DELMAS, A. MAAZAZ, C. FOUASSIER, J. M. REAU, AND P. HAGENMULLER, *in* "Proceedings of the Conference 'Fast Ion Transport in Solids,' Lake Geneva, USA," p. 451 (1979).